Rad-hard properties of the optical glass adopted for the PLATO space telescope refractive components

ALAIN JODY CORSO,[1,*] ENRICO TESSAROLO,[1] STEFANIA BACCARO,[2] ALESSIA CEMMI,[2] ILARIA DI SARCINA,[2] DEMETRIO MAGRIN,[3] FRANCESCO BORSA,[4] ROBERTO RAGAZZONI,[3] VALENTINA VIOTTO,[3] ANDREA NOVI,[5] MATTEO BURRESI,[5] FRANK PELLOWSKI,[6] MARIO SALATTI,[7] ISABELLA PAGANO,[8] AND MARIA GUGLIELMINA PELIZZO[1,9,10]

[1]National Research Council of Italy – Institute for Photonics and Nanotechnologies Padova, Via Trasea 7, 35131 Padova, Italy
[2]Department for Fusion and Nuclear Safety Technologies, ENEA, Via Anguillarese 301, 00123 Rome, Italy
[3]INAF – Osservatorio Astronomico di Padova, Vicolo dell'Osservatorio 5, 35122 Padova, Italy
[4]INAF – Osservatorio Astronomico di Brera, Via E. Bianchi 46, 23807 Merate (LC), Italy
[5]Leonardo S.p.A. Airborne & Space System Div. - Via delle Officine Galileo 1, Campi Bisenzio (FI), 50013, Italy
[6]OHB System, Manfred-Fuchs-Straße 1, 82234 Weßling – Oberpfaffenhofen, Germany
[7]ASI – Agenzia Spaziale Italiana, via del Politecnico snc, 00133 Rome, Italy
[8]INAF – Osservatorio Astrofisico di Catania, via Santa Sofia 78, 95123 Catania, Italy
[9]Department of Information Engineering, University of Padova, Via Gradenigo 6B, 35131 Padova, Italy
[10]pelizzo@dei.unipd.it
*alain.corso@pd.ifn.cnr.it

Abstract: PLAnetary Transits and Oscillations of stars (PLATO) is a medium sized mission (M3) selected by the European Space Agency (ESA) for launch in 2026. The PLATO payload includes 26 telescopes all based on a six-element refractive optical scheme. Some components will be eventually manufactured by S-FPL51, N-KZFS11 and S-FTM16 glass whose radiation resistance is partially or totally unknown. The radiation-resistance properties of such materials have been investigated by using a ^{60}Co γ-rays source as probe. Each optical component has been characterized by a depth profile curve which describes the transmission loss as a function of the thickness in dependence of the impinging dose. A model to simulate the throughput of the whole instrument has been developed and used to verify the instrument performance considering different stellar spectra.

1. Introduction

The project PLAnetary Transits and Oscillations of stars (PLATO) is a medium size mission (M3) selected by the European Space Agency (ESA) in the framework of the Cosmic Vision 2015-2025 program for launch in 2026. The satellite will operate in the Lagrangian point L2 and a minimum mission lifetime of 4.5 years is expected. The main science goal of PLATO is to discover and characterize extrasolar planets, including terrestrial planets in the habitable zone; such goal will be achieved through high-precision, long-term (up to three years) photometric and asteroseismic monitoring of a large number of bright stars. For each planet the radius, the mass (in synergy with ground-based follow-up) and the age will be determined with unprecedented accuracy, making PLATO able to deliver the first large-scale catalogue of well-characterized small planets at intermediate orbital periods [1].

The PLATO payload includes 24 cameras, which will perform photometric measurements in the 500-1000 nm wavelength range. Moreover, in the same optical bench two additional

fast cameras operating in different photometric bands (blue 500-675 nm, red 675-1000 nm) will be devoted to improve the pointing stability performance of the spacecraft. Each camera is based on the same optical scheme (see Fig. 1(a)), called Telescope Optical Unit (TOU). The design of the TOU [2] has been mainly driven by performance requirements and mass budget. The selected configuration is a fully refractive optical system made of six lenses and a window placed at the entrance of the objective. The optical solution is able to match the required performance with a limited mass budget. This configuration is a refractive wide field system (about 38 degrees) with an entrance pupil diameter of 120 mm. In order to achieve the required performance keeping mass as low as possible, to locate the pupil at the center of the optical layout is a mandatory choice. The results is a modified Double-Gauss configuration in which the last lens (L6) acts as a field flattener. In order to achieve an adequate chromatic correction, a combination of glasses having a high Abbe number, such as CaF_2 or S-FPL51, together with flint glasses, which are not radiation hardened, are required. Moreover, because CaF_2 is highly sensitive to thermal shocks, this material was selected for the lens placed in the central position (L3), well protected against the electronic power dissipation of the CCDs on one side and the outer space on the other. Since most of the glasses are not radiation resilient, a Suprasil window has been introduced in order to protect them by the incoming radiations, decreasing the total dose absorbed by the following elements. Although it was not deliberately on the design constraints, such combination of glasses results in a significant robust system stable against thermal deterioration of the optical performance.

As mentioned before, the TOU window will be manufactured by Suprasil while lens L3 by CaF_2: both these materials are naturally radiation resistant glass suitable for space applications [3–5]. Lens L6 will be made by the Ce-doped glass BK7G18, which have been proven to have a high resistance to radiation [5–7]. On the contrary, very little is known on the radiation-resistance properties of the glass designated for lenses L1, L4 (S-FPL51, Ohara) and L5 (S-FTM16, Ohara) [8,9] and none about the glass of lens L2 (N-KZFS11, Schott). Considering that for mass reduction purposes the mechanical tube surrounding the lenses is made in AlBeMet (Fig. 1(b)), which provides extraordinary mechanical properties but low radiation shielding capability (about 1/3 with respect to aluminum), it becomes pivotal for the mission to investigate the radiation-resistance properties of S-FPL51, S-FTM16, and N-KZFS11 glasses.
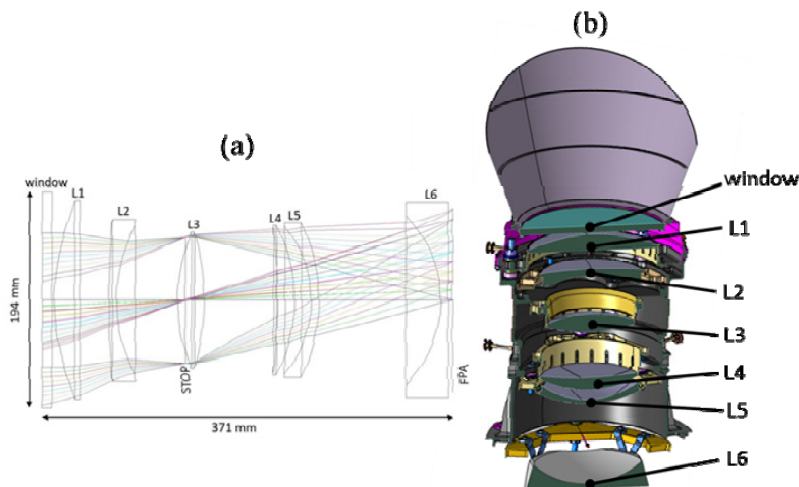

Fig. 1. Layout of the TOU: (a) optical layout and (b) cutaway view of the opto-mechanical layout.

The radiative environmental parameters of the PLATO mission are reported in the ESA "Plato Environmental Specification" issue [10]. It is expected that the main contribution to

the total ionizing dose undergone by PLATO will come from the solar protons whose spectrum at the Lagrangian point L2 can be estimated by the SPace ENVironment Information System (SPENVIS) [11]. Considering the attenuation provided by the TOU sector shielding, the worst-case surface doses expected on each of the PLATO lenses after 6.5 years mission lifetime are reported in Table 1.

Table 1. Worst-case surface doses expected after 6.5 years mission on the PLATO lenses.

Lens	Glass	Density (g/cm^3)	Dose (krad)	Dose (Gy)
Window	Suprasil	2.20	608.8	6088
L1	S-FPL51	3.62	7.4	74
L2	N-KZFS11	3.20	2.9	29
L3	CaF$_2$	3.18	2.4	24
L4	S-FPL51	3.62	1.7	17
L5	S-FTM16	2.64	10.5	105
L6	BK7-G18	2.52	616.5	6165

In order to evaluate the resistance of S-FPL51, N-KZFS11 and S-FTM16 glasses to such doses, γ-rays were used to investigate the induced ionizing effects. The main advantage of this approach is that the γ-rays ensure a uniform energy release inside the tested components such that the ionizing dose effects can be easily decoupled from the thickness of the used samples. In this way, the darkening properties of each glass were determined in term of the radiation-induced absorption coefficient [12].

The results obtained by the γ-rays irradiation tests were used to evaluate the impact of the mission environment on the TOU performance. Taking into account the shielding properties given by the current TOU optical-mechanical scheme, the darkening induced by the Lagrangian point L2 proton spectra was evaluated for each optical element after a mission lifetime of 6.5 years. Finally, the changes expected on of the instrumental performance was estimated for targets with different stellar temperatures.

2. Irradiation test with γ-rays

2.1 Material and methods

The glass investigated in this work and their main chemical ingredients are listed in Table 2. V1 is a fluorophosphate glass rich of alkaline earth fluorides. V2 is a borosilicate glassy matrix doped with transition metals oxides while V3 is a silicate glass enriched of Ti oxide. For each glass, three different disks specimen with a diameter of 12 mm were fabricated. The thickness of the specimens is reported in Table 2.

Table 2. List of glasses tested.

Sample label	Glass type	Specimen thickness (mm)
V1	S-FPL51 (OHARA)	3.10 ± 0.05
V2	N-KZFS11 (SCHOTT)	3.20 ± 0.05
V3	S-FTM16 (OHARA)	3.60 ± 0.05

Gamma irradiation was performed at the ^{60}Co *Calliope* facility at ENEA Casaccia Research Center, Rome (Italy) [13]. The emitted radiation consists of γ-rays at 1.17 MeV and 1.33 MeV, with a mean photon's energy of 1.25 MeV. The irradiation was performed in air, at room temperature and in the dark in order to avoid unwanted recovery processes induced by the visible light. The tests were carried out at four dose rates, namely LLDR = 7.3 krad$_{Si}$/h (1 specimen for each glass), LDR = 14.7 krad$_{Si}$/h (1 specimen for each glass), MDR = 27.3 krad$_{Si}$/h (1 specimen for each glass) and HDR = 116.8 krad$_{Si}$/h (1 specimen for each glass). The dose rates were experimentally determined by Fricke absolute dosimetry (error of 3%) [13], while the total absorbed doses were derived taking into account the irradiation session

duration. The irradiation was performed in step doses (Table 3) and the optical transmittance T of the samples was measured before and immediately after each irradiation step by using a double-beam spectrophotometer Perkin Elmer Lambda 950 in the 200-2000 nm wavelength range. The accuracy on the T measurements, including also the sample misalignment, was 1.3%. Optical transmittance T is related to the linear absorption coefficient, named α, by the Lambert–Beer law

$$\ln T = -\alpha d \tag{1}$$

where d is the sample thickness expressed in cm. The γ-rays induced darkening can be computed using the relative radiation-induced absorption coefficient μ, defined as

$$\mu_D = \frac{1}{d} \ln\left(\frac{T_0}{T_D}\right) = \alpha_D - \alpha_0 \tag{2}$$

where T_0 and T_D are the sample transmittances before and immediately after the irradiation at dose D. As expressed in Eq. (2), the μ coefficient provides the variation of the absorption coefficient and it is proportional to the density of the color centers induced in the glass matrix [5].

Table 3. Absorbed dose steps in which the samples were characterized.

Step	Absorbed dose LLDR ($krad_{Si}$)	Absorbed dose LDR ($krad_{Si}$)	Absorbed dose MDR ($krad_{Si}$)	Absorbed dose HDR ($krad_{Si}$)
1	5.1	10.3	35.5	52.0
2	10.2	44.4	129.4	103.9
3	40.3	267.8	560.0	305.9
4	134.9	331.3	1061.8	500.0
5	276.7	563.0	2999.6	1986.2
6	426.7	862.8		
7		1892.5		

2.2 Irradiation results

UV–VIS–NIR transmittance spectra before the LLDR and LDR irradiation (black dashed line) and immediately after each irradiation step (colored solid lines) are reported in Fig. 2. Similar curves were obtained for the MDR and HDR (not reported in this paper).
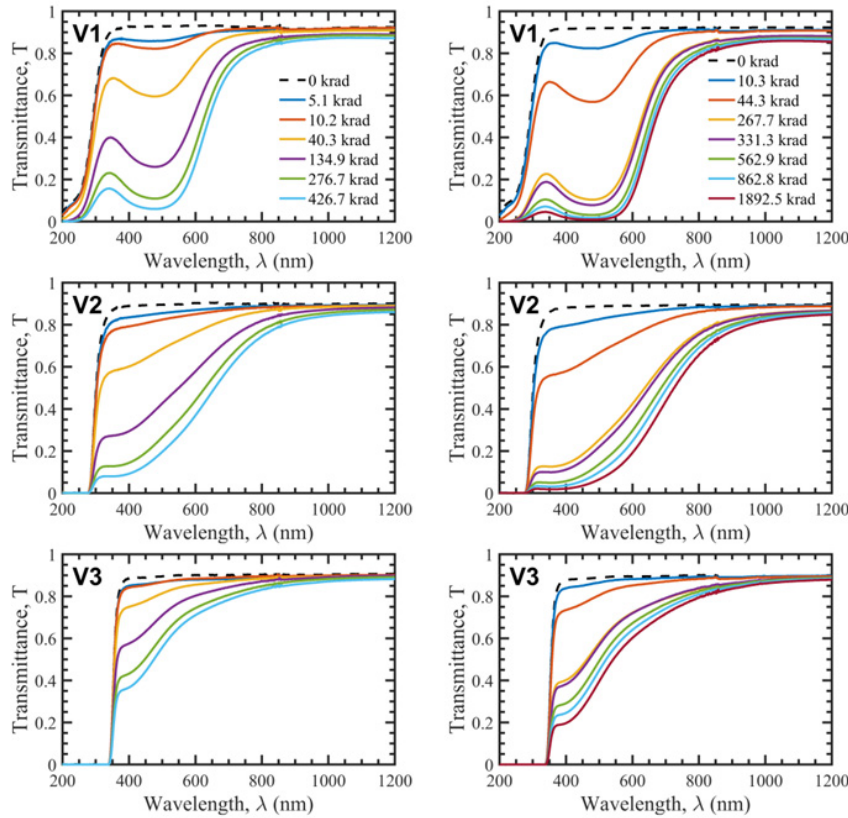
Fig. 2. Transmittance spectra of the glass samples before (dashed curves) and after each irradiation step at LLDR (left column) and LDR (right column).

As expected, these spectra show that γ-ray irradiation causes a general decrease of the transmittance in the UV and VIS range due to the formation of defects in the glass structure. In particular, two different kind of defects can be created in the glassy matrices: hole centers (HCs), captured by anions near cation vacancies, and electron centers (ECs) located in anion vacancies; ECs absorb in ultraviolet region while HCs absorb in the visible range [14,15].

The transmittance curves of the analyzed samples present different cut-off edge positions and absorption behavior. Depending on the main chemical components of the glassy matrix, a gradual red-shift of the cut-off edge is evident (before and after irradiation), from around 220 nm (fluorphosphate matrix, V1), to around 300 nm (borosilicate matrix, V2) and to around 350 nm (silicate glass, V3) [15–17].

The growth of the radiation-induced absorption coefficient as a function of the absorbed dose at a specific wavelength can be described by the following relationship:

$$\mu(\lambda, D) = N_C(\lambda)D + \sum_{j=1}^{m} N_j(\lambda)(1 - e^{-\frac{D}{\delta_j(\lambda)}}) \tag{3}$$

which is a generalization of the models previously presented by Levy et al. [18], Galeener et al. [19] and Mashkov et al. [20]. The term N_C describes the creation of defects which linearly depend on the absorbed dose D. Given m as the number of precursors in the glass matrix, the sum of the exponential terms describes the activation effects; in this specific case, the fit is satisfying by using one exponential term ($m = 1$). The radiation-induced absorption curve as

function of the dose was retrieved by fitting the data measured at $\lambda = 500$ nm, $\lambda = 600$ nm and $\lambda = 700$ nm; such wavelengths were selected considering that PLATO will observe above 500 nm and that the glass degradation above 700 nm starts to be small (see Fig. 3 for LLDR case, Fig. 4 for LDR, Fig. 5 for MDR and Fig. 6 for HDR).
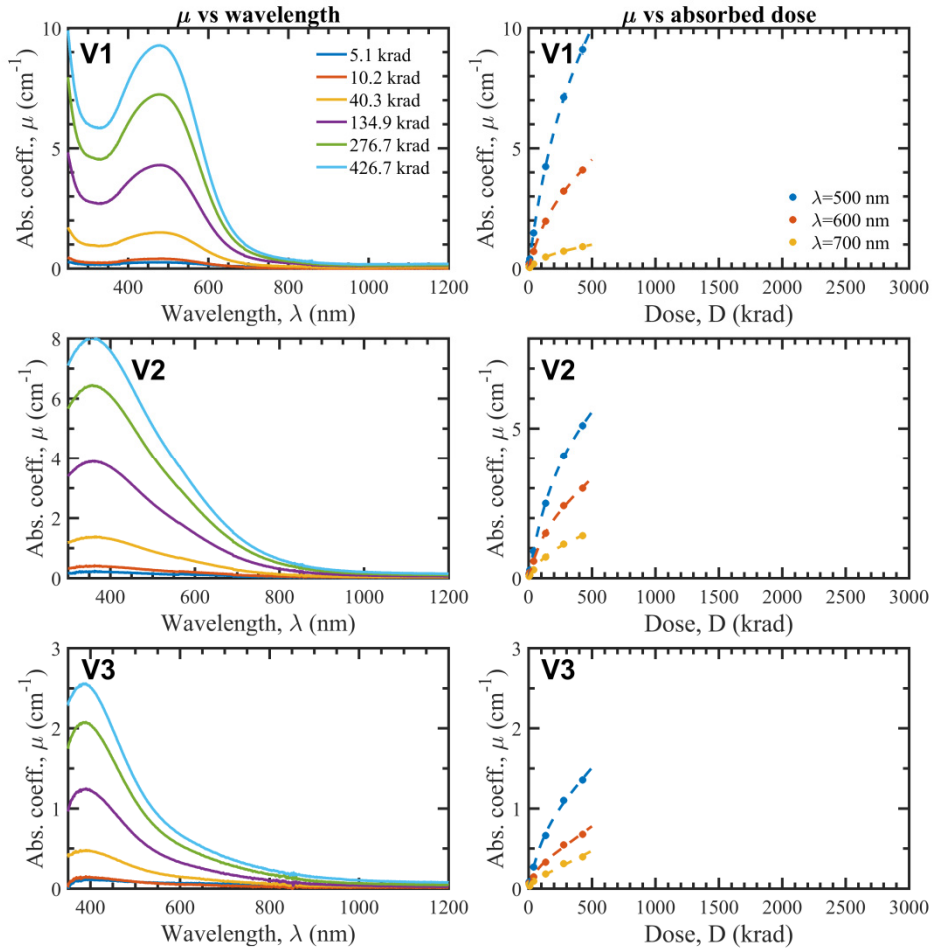

Fig. 3. On the left column: the relative radiation-induced absorption coefficient μ computed for the sample irradiated with the LLDR. On the right column: experimental induced absorption coefficient μ (dots) at $\lambda = 500$ nm, $\lambda = 600$ nm and $\lambda = 700$ nm for the irradiation with the LLDR. The best fit obtained with the Eq. (3) is also reported (dashed lines). In Eq. (3), only one exponential term was considered (m = 1).
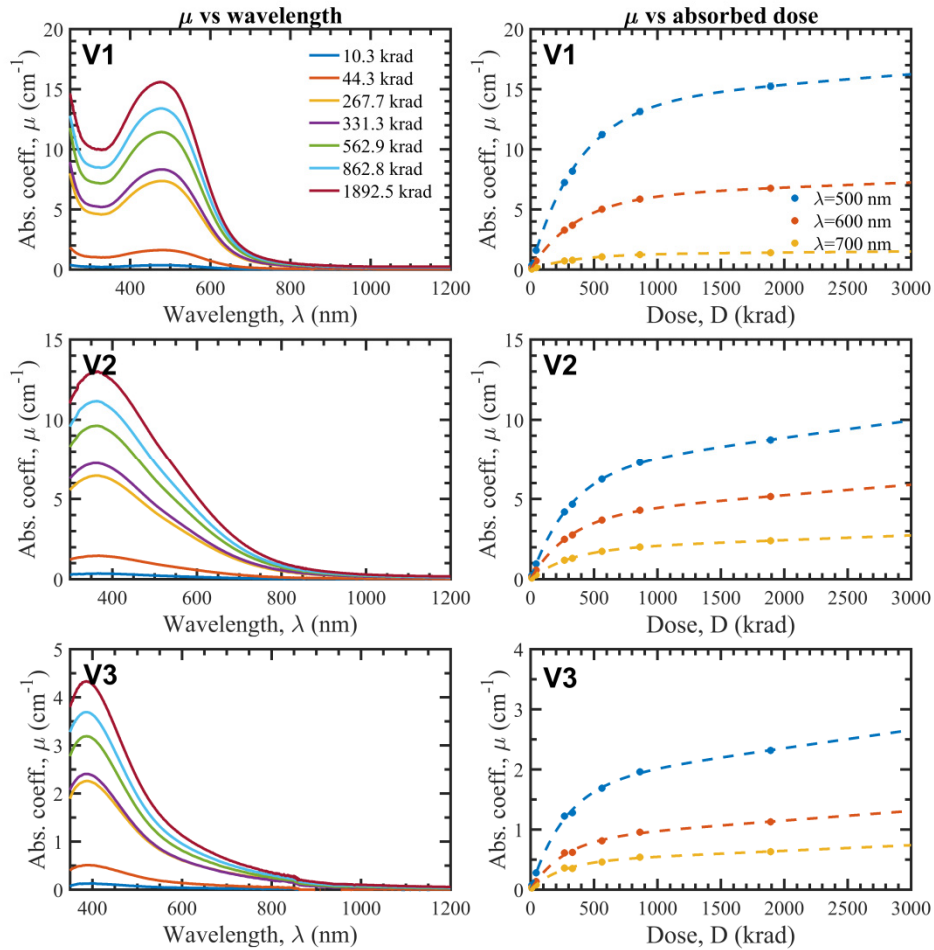
Fig. 4. On the left column: the radiation-induced absorption coefficient μ computed for the sample irradiated at LDR. On the right column: radiation-induced absorption coefficient μ (dots) at $\lambda = 500$ nm, $\lambda = 600$ nm and $\lambda = 700$ nm for the irradiation at LDR. The best fit obtained with the Eq. (3) is also reported (dashed lines). In Eq. (3), only one exponential term was considered ($m = 1$).
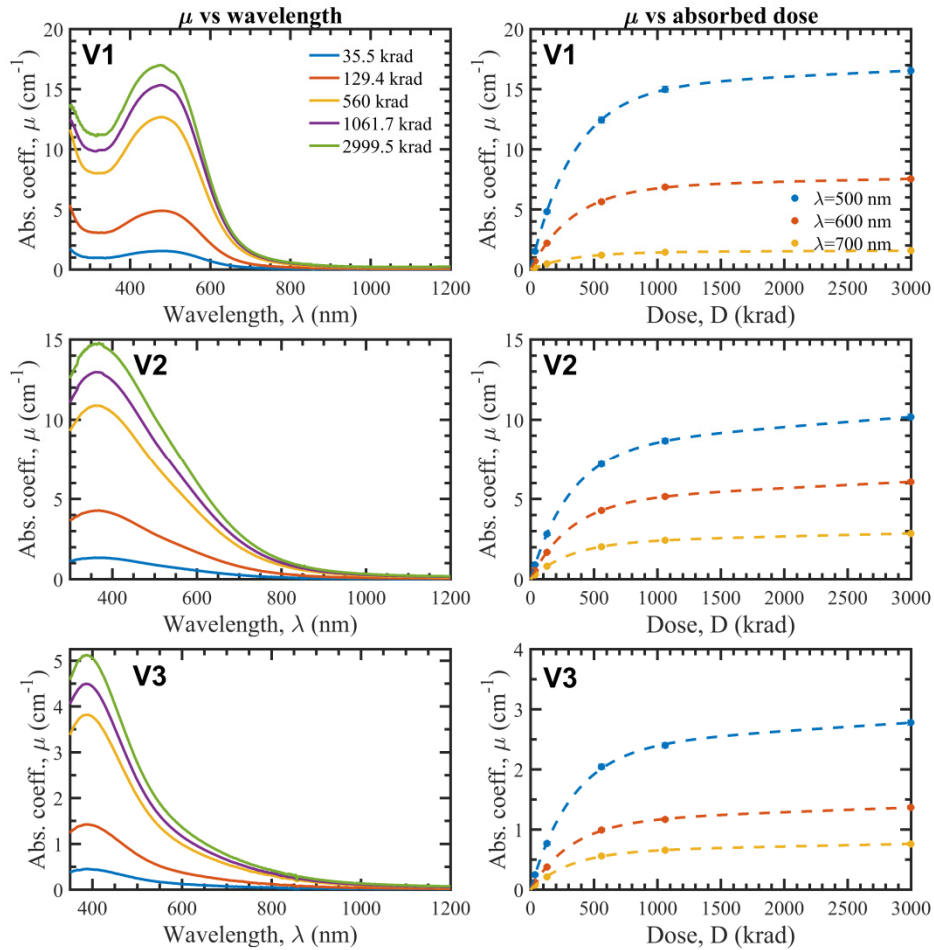
Fig. 5. On the left column: the relative radiation-induced absorption coefficient μ computed for the sample irradiated with the MDR. On the right column: experimental induced absorption coefficient μ (dots) at $\lambda = 500$ nm, $\lambda = 600$ nm and $\lambda = 700$ nm for the irradiation with the MDR. The best fit obtained with the Eq. (3) is also reported (dashed lines). In Eq. (3), only one exponential term was considered (m = 1).
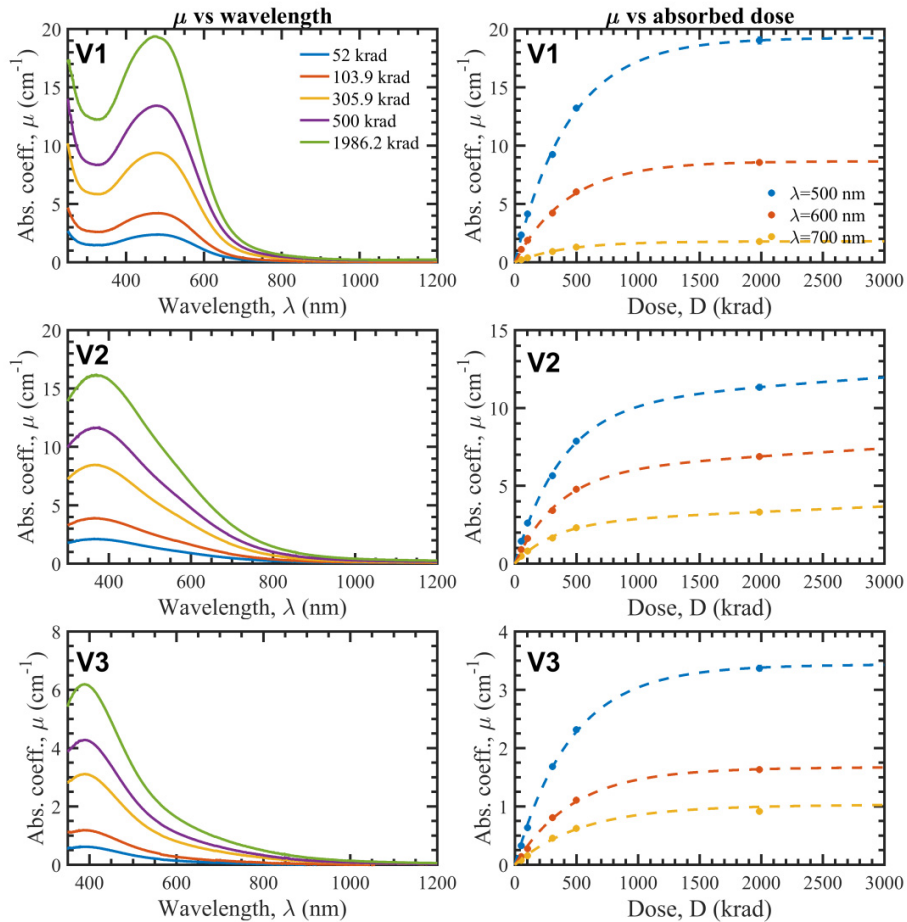
Fig. 6. On the left column: the relative radiation-induced absorption coefficient μ computed for the sample irradiated with the HDR. On the right column: experimental induced absorption coefficient μ (dots) at λ = 500 nm, λ = 600 nm and λ = 700 nm for the irradiation with the HDR. The best fit obtained with the Eq. (3) is also reported (dashed lines). In Eq. (3), only one exponential term was considered (m = 1).

Moreover, the μ-curves reported in the left column of Figs. 3, 4, 5 and 6, proves that the absorption induced after γ-ray irradiation depends on the different composition of the investigated glasses. V1 and V2 matrices show lower radiation hardness, with more pronounced absorption than V3 glass. In particular, the addition of high amount of oxides with large cation sizes (Na, Ta, Zr) in the V2 borosilicate matrix, induces a severe modification of the glass structure, resulting in the formation of non-bonding oxygen sites (NBOs), able to absorb in the visible range (HCs defects) [17,21,22]. Considering the V3 matrix, the titanium oxide addition improves its radiation hardness especially in the UV region, due to the recombination of ECs with Ti(IV) that is reduced to Ti(III). The increasing amount of Ti(III), however, is responsible of new HCs defects formation which absorb near 500-550 nm [23].

The radiation-induced absorption appears to be dependent on the dose rate, as shown in Fig. 7. During irradiation, a higher dose-rate systematically corresponds to a greater absorption coefficient and then to a higher concentration of UV absorbing centers; the difference is already evident for doses above 100 krad. This dose rate dependence is due to

the high efficiency of the color centers recombination process: in fact, in the case the recombination time is comparable with duration of the γ-rays irradiation test, the lower is the dose rate the greater is the effect of the centers recombination in the absorption coefficient.

For doses lower than 100 krad, Eq. (3) can be approximated using a truncated Taylor's series:

$$\mu(\lambda,\ \mathrm{D}) \approx \left(N_C(\lambda) + \frac{N_1(\lambda)}{\delta_1(\lambda)} \right) D = k(\lambda)D \quad \text{for} \quad D \ll \sqrt{6}\delta_1(\lambda) \quad (4)$$

where k is the linear radiation-induced absorption coefficient. By fitting the μ experimental curves with Eq. (3), the linear absorption coefficient k versus wavelength of a sample can be obtained for each dose rate. Figure 7 reports such coefficients for each sample. As expected, a dependence on the dose rate is still present since, as discussed, at a specific deposited dose the dose-rate determines the number of color centers and defects formed during the irradiation.
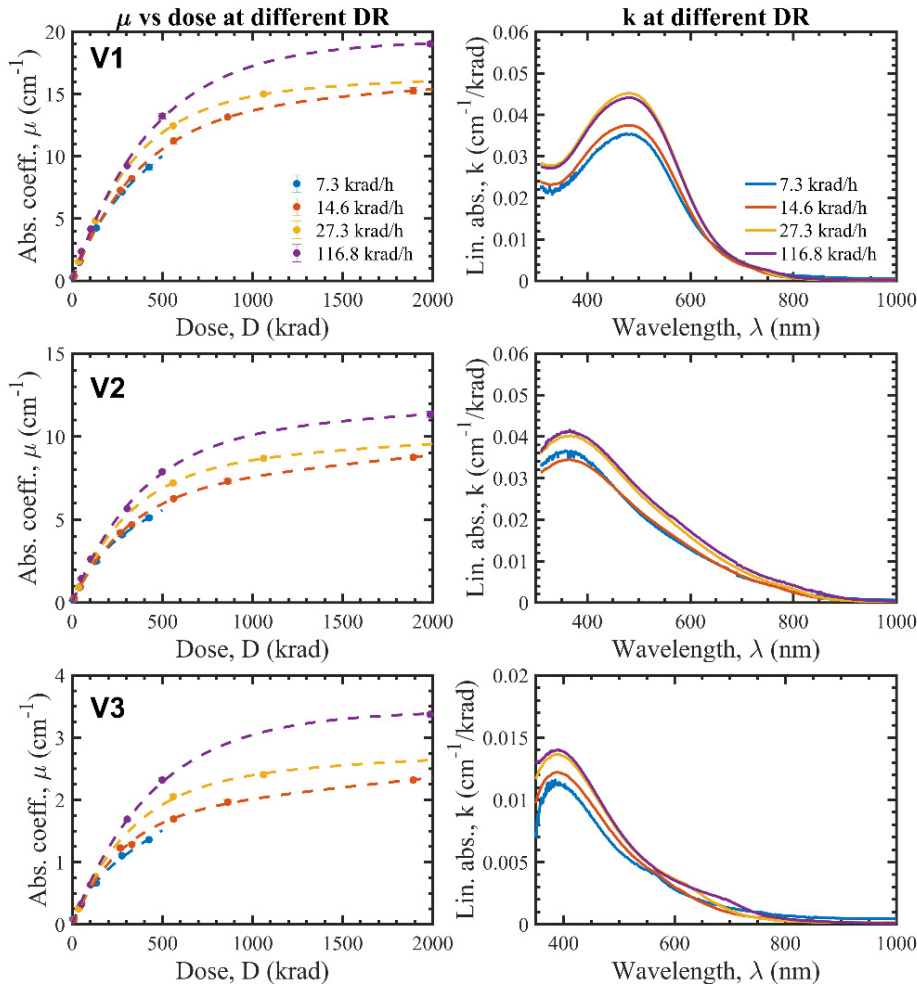

Fig. 7. On the left column: radiation-induced absorption coefficient μ at λ = 500 nm obtained at the four dose rates considered in this work. On the right column: linear radiation-induced absorption coefficient k versus wavelength retrieved from the experimental measurements at the four dose rates considered in this work.

3. Impact on PLATO TOU

The irradiation tests were performed in order to study the rad-hard properties of some of the glass of PLATO telescope, for which no/poor information was available. With these results, a quantification of the transmission loss of each lens after the exposure in the Lagrange point environment can be estimated.

The radiation spectra affecting each lens of the TOU were retrieved using the reference proton spectrum expected in the Lagrange point as input [10]. MULASSIS [24] and FASTRAD [25] codes were used to calculate the average proton fluence impinging on each lens, taking into account the TOU geometry and the shielding effects given by the AlBeMeT tube structure (see Fig. 8).
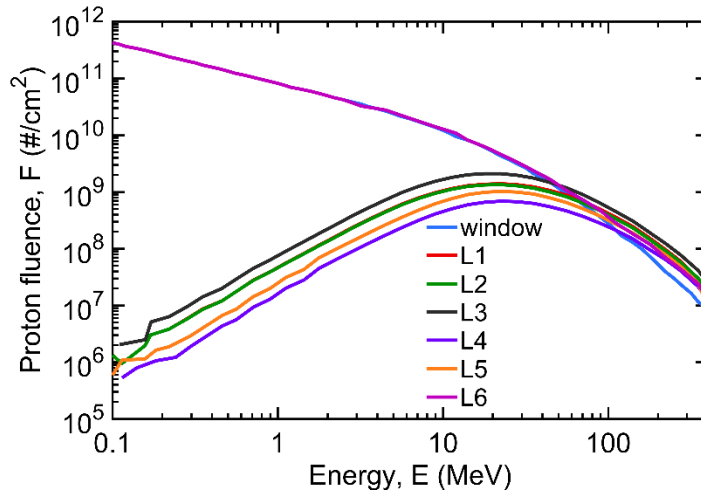

Fig. 8. The integral proton fluence spectra impinging at each lens. The fluence spectrum of L6 and of the TOU window has the same shape of that of the Lagrangian point environment because such components are unshielded by the AlBeMeT tube.

Unlike the case of γ-rays in which the energy is uniformly released along the thickness of an optical component, low energy protons release the energy inside the component by following a precise dose-depth profile. Such curves were estimated for each TOU component by adopting an equivalent aluminium shielding thicknesses model. Starting from the proton fluences reported in Fig. 8, the Shieldose2 code [26] was used to compute the ionizing dose deposited along the thickness of a semi-infinite reference aluminium slab. Afterwards, this dose-depth profile was used to compute the equivalent curve in other materials by following the relationship

$$D_2\left(t_2\right) = D_{Al}\left(\frac{\rho_2}{\rho_{Al}}t_2\right) \tag{5}$$

where D, t and ρ are the dose, thickness and density, respectively. Figure 9 reports the dose-depth profiles, normalized for the surface dose, which were computed considering the densities reported in Table 1. Thus, knowing the local surface dose and the dose-depth profile, the total ionizing dose can be computed.
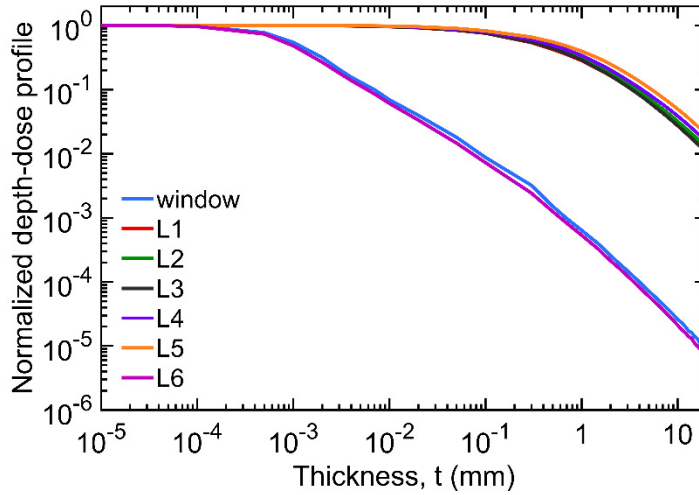
Fig. 9. Normalized dose-depth computed for each component of PLATO TOU.

The transmittance drop undergoes by each lens can be obtained by discretizing into N layers the portion of the glass affected by the ionizing radiation and evaluating the transmission loss within each layer according to the local absorbed dose. The darkening occurring in the $i-$ th layer is given by [27]:

$$\frac{T_i}{T_{0i}} = e^{-k(\lambda)D_i x_i} \tag{6}$$

where T_{0i} is the transmittance of the $i-$ th layer before the irradiation, D_i is the average dose absorbed by the $i-$ th layer and x_i is the layer thickness. In Fig. 10 an example of the transmittance drop expected at 500 nm wavelength as a function of depth is reported for each component material up to 10 mm thickness. The k values used in the simulations were those obtained at the LLDR for the three glasses; for the remaining materials, the k values were retrieved from the data available in literature [4–6].
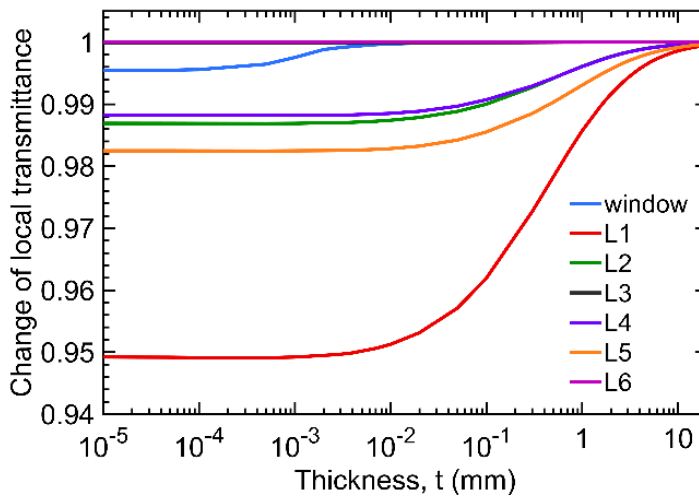

Fig. 10. Example of local transmission change after worst case irradiation @500nm as a function of depth. The darkening is concentrated in the first layers of glass after the surface.

Based on the results in Fig. 10, L1 is the optical element undergoing the higher darkening because of the high absorption coefficient found for S-FPL51 glass. Instead, the degradation expected for the components L2, L4 and L5 is lower, mainly because such components are better shielded from the radiating environment (Table 1 reports the doses estimated for each component). No degradation in transmittance is expected for the component L3 due to the high shielding and the high radiation resistance offered by this material [5]. L6 lens, which is not shielded, will be exposed at the same doses of the Suprasil windows (see Table 1). Despite the high doses deposited on the Suprasil window, the absorption coefficient expected for this material is relatively low [5] and consequentially a slightly darkening is expected. Finally, as L6 will be manufactured with a Ce-doped glass (BK7-G18) which shows no degradation for doses up to 5Mrad [6], no transmission change is expected for the doses foreseen during the PLATO operation.

To evaluate the total transmission loss for each component, the following formula has been used:

$$\prod_{i=1}^{N} \frac{T_i}{T_{0i}} = e^{-k(\lambda)\sum_{i=1}^{N} D_i x_i} = e^{-k(\lambda)D_{eq}} \tag{7}$$

where D_{eq} takes the meaning of equivalent average dose.

In order to simulate changing of the performance of the telescope during it lifetime, the results obtained for each single component have been combined by calculating the transmission loss along the path of rays coming from an on-axis point source placed at infinity and passing through 5 points on the entrance pupil (i.e. the center one, and four equally distributed points on an external ring). In Fig. 11, the averaged curve showing the percentage of transmission loss of each component and the full telescope are reported for a 6.5 years lifetime of the PLATO mission; a radiation margin RDM = 2 has been taken into account.
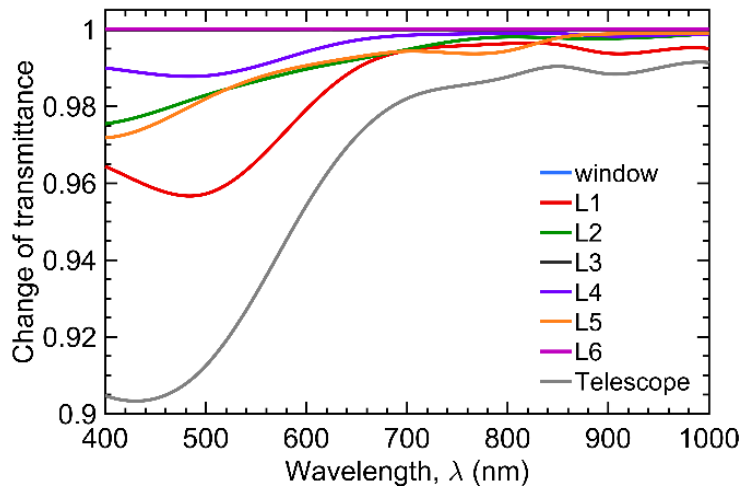

Fig. 11. Simulated transmission change of each lens for the PLATO telescopes vs. wavelength after 6.5 years in orbit. A dose margin RDM = 2 has been considered.

Since PLATO is conceived to perform photometric measurement on stars, results have to be interpreted considering their impact on the observation of various stellar spectra. Since blackbody temperatures in between 5500 and 6500 K are expected in 90% of the PLATO targets, the percentage of signal loss has been evaluated considering the correspondent simulated stellar spectra. The values are presented in Table 4.

Table 4. Signal loss after 6.5 years in orbit for three different stellar temperatures considering a RDM = 2.

Stellar Temperature	Signal loss
5500 K	−3.49%
6000 K	−3.62%
6500 K	−3.74%

4. Conclusions

S-FPL51, N-KZFS11 and S-FTM16 glass resistance properties have been investigated by using a ^{60}Co γ-rays source. Various step doses achieved at four different dose rates were considered. The samples have been characterized in term of transmittance. Results show that γ-rays induce colors with an overall degradation of the efficiency for wavelengths shorter than 700 nm. The radiation-induced absorption coefficient μ associated to the color centers was found to be dependent on the dose rate for a given absorbed dose.

The results obtained by the γ-rays irradiation tests have been used to evaluate the impact of the mission environment on the PLATO telescopes performance. Considering that the main contribution of the environmental radiation comes from solar protons, the total dose-depth profile and the consequent darkening have been estimated for each telescope lens. Such simulations were performed taking into account the shielding properties given by the current optical-mechanical scheme. It was found that after a mission lifetime of 6.5 years, the expected instrumental efficiency degradation is limited to 3.5%.

Funding

Acknowledgments

References

1. H. Rauer, C. Catala, C. Aerts, T. Appourchaux, W. Benz, A. Brandeker, J. Christensen-Dalsgaard, M. Deleuil, L. Gizon, M. J. Goupil, M. Güdel, E. Janot-Pacheco, M. Mas-Hesse, I. Pagano, G. Piotto, D. Pollacco, Ċ. Santos, A. Smith, J. C. Suárez, R. Szabó, S. Udry, V. Adibekyan, Y. Alibert, J. M. Almenara, P. Amaro-Seoane, M. Ammler-von Eiff, M. Asplund, E. Antonello, S. Barnes, F. Baudin, K. Belkacem, M. Bergemann, G. Bihain, A. C. Birch, X. Bonfils, I. Boisse, A. S. Bonomo, F. Borsa, I. M. Brandão, E. Brocato, S. Brun, M. Burleigh, R. Burston, J. Cabrera, S. Cassisi, W. Chaplin, S. Charpinet, C. Chiappini, R. P. Church, S. Csizmadia, M. Cunha, M. Damasso, M. B. Davies, H. J. Deeg, R. F. Díaz, S. Dreizler, C. Dreyer, P. Eggenberger, D. Ehrenreich, P. Eigmüller, A. Erikson, R. Farmer, S. Feltzing, F. de Oliveira Fialho, P. Figueira, T. Forveille, M. Fridlund, R. A. García, P. Giommi, G. Giuffrida, M. Godolt, J. Gomes da Silva, T. Granzer, J. L. Grenfell, A. Grotsch-Noels, E. Günther, C. A. Haswell, A. P. Hatzes, G. Hébrard, S. Hekker, R. Helled, K. Heng, J. M. Jenkins, A. Johansen, M. L. Khodachenko, K. G. Kislyakova, W. Kley, U. Kolb, N. Krivova, F. Kupka, H. Lammer, A. F. Lanza, Y. Lebreton, D. Magrin, P. Marcos-Arenal, P. M. Marrese, J. P. Marques, J. Martins, S. Mathis, S. Mathur, S. Messina, A. Miglio, J. Montalban, M. Montalto, M. J. P. F. G. Monteiro, H. Moradi, E. Moravveji, C. Mordasini, T. Morel, A. Mortier, V. Nascimbeni, R. P. Nelson, M. B. Nielsen, L. Noack, A. J. Norton, A. Ofir, M. Oshagh, R. M. Ouazzani, P. Pápics, V. C. Parro, P. Petit, B. Plez, E. Poretti, A. Quirrenbach, R. Ragazzoni, G. Raimondo, M. Rainer, D. R. Reese, R. Redmer, S. Reffert, B. Rojas-Ayala, I. W. Roxburgh, S. Salmon, A. Santerne, J. Schneider, J. Schou, S. Schuh, H. Schunker, A. Silva-Valio, R. Silvotti, I. Skillen, I. Snellen, F. Sohl, S. G. Sousa, A. Sozzetti, D. Stello, K. G. Strassmeier, M. Švanda, G. M. Szabó, A. Tkachenko, D. Valencia, V. Van Grootel, S. D. Vauclair, P. Ventura, F. W. Wagner, N. A. Walton, J. Weingrill, S. C. Werner, P. J. Wheatley, and K. Zwintz, "The PLATO 2.0 mission," Exp. Astron. **38**(1–2), 249–330 (2014).
2. D. Magrin, R. Ragazzoni, M. Bergomi, F. Biondi, S. Chinellato, M. Dima, J. Farinato, D. Greggio, M. Gullieuszik, L. Marafatto, V. Viotto, M. Munari, I. Pagano, D. Sicilia, S. Basso, F. Borsa, M. Ghigo, D. Spiga, T. Bandy, M. Brändli, W. Benz, G. Bruno, T. De Roche, D. Piazza, M. Rieder, A. Brandeker, M. Klebor, V. Mogulsky, M. Schweitzer, M. Wieser, A. Erikson, and H. Rauer, "Manufacturing and alignment tolerance analysis through Montecarlo approach for PLATO," Proc. SPIE **9904**, 99042Z (2016).
3. C. D. Marshall, J. A. Speth, and S. A. Payne, "Induced optical absorption in gamma, neutron and ultraviolet irradiated fused quartz and silica," J. Non-Cryst. Solids **212**(1), 59–73 (1997).

4. I. Di Sarcina, M. L. Grilli, F. Menchini, A. Piegari, S. Scaglione, A. Sytchkova, and D. Zola, "Behavior of optical thin-film materials and coatings under proton and gamma irradiation," Appl. Opt. **53**(4), A314–A320 (2014).

5. T. D. Henson and G. K. Torrington, "Space radiation testing of radiation-resistant glasses and crystals," Proc. SPIE **4452**, 54–65 (2001).

6. S. Baccaro, A. Cemmi, I. Di Sarcina, and F. Menchini, "Gamma rays effects on the optical properties of Cerium-doped glasses," Int. J. Appl. Glass Sci. **6**(3), 295–301 (2015).

7. A. I. Gusarov, D. Doyle, A. Hermanne, F. Berghmans, M. Fruit, G. Ulbrich, and M. Blondel, "Refractive-index changes caused by proton radiation in silicate optical glasses," Appl. Opt. **41**(4), 678–684 (2002).

8. K. B. Miller, J. Leitch, and C. Lyons-Mandel, "Proton radiation testing of optical elements," in Proceedings of IEEE Radiation Effects Data Workshop, (IEEE 2001) pp. 155–159.

9. F. Grupp, N. Geis, R. Katterloher, and R. Bender, "Radiation damage to six selected optical materials," Proc. SPIE **8860**, 88600N (2013).

10. European Space Agency, "Plato Environmental Specification," (2012).

11. European Space Agency, "SPENVIS - Space environment information system," https://www.spenvis.oma.be/ (lastaccess in November 2018).

12. Y. Ou, S. Baccaro, Y. Zhang, Y. Yang, and G. Chen, "Effect of gamma-ray irradiation on the optical properties of PbO–B_2O_3–SiO_2 and Bi_2O_3–B_2O_3–SiO_2 glasses," J. Am. Ceram. Soc. **93**(2), 338–341 (2010).

13. S. Baccaro, A. Cemmi, G. Ferrara, and S. Fiore, "Calliope gamma irradiation facility at ENEA – Casaccia R.C. (Rome)," ENEA Report RT/2015/13/ENEA (2015).

14. E. J. Friebele, "Radiation effects," in Optical properties of glass (American Ceramic Society, 1991), pp. 205–262.

15. D. Ehrt and W. Vogel, "Radiation effects in glasses," Nucl. Instrum. Methods Phys. Res. B **65**(1–4), 1–8 (1992).

16. S. Baccaro, A. Cecilia, A. Cemmi, E. Mihokova, M. Nikl, K. Nitsch, P. Polato, G. Zanella, and R. Zannoni, "Color centers induced by gamma irradiation in scintillating glassy matrices for middle and low energy physics experiments," Nucl. Instrum. Methods Phys. Res. B **185**(1–4), 294–298 (2001).

17. Y. Ou, S. Baccaro, Y. Zhang, Y. Yang, and G. Chen, "Effect of gamma-ray irradiation on the optical properties of PbO-B2O3-SiO2 and Bi2O3- B2O3-SiO2 glasses," J. Am. Ceram. Soc. **93**(2), 338–341 (2010).

18. P. W. Levy, P. L. Mattern, K. Lengweiler, and M. Goldberg, "Studies on nonmetals during irradiation: IV — The effect of strain applied during irraldition on the gamma-ray-induced F-center coloring of KCl at room temperature," Solid State Commun. **9**(22), 1907–1912 (1971).

19. F. L. Galeener, D. B. Kerwin, A. J. Miller, and J. C. Mikkelsen, Jr., "X-ray creation and activation of electron spin resonance in vitreous silica," Phys. Rev. B Condens. Matter **47**(13), 7760–7779 (1993).

20. V. A. Mashkov, W. R. Austin, L. Zhang, and R. G. Leisure, "Fundamental role of creation and activation in radiation-induced defect production in high-purity amorphous SiO_2," Phys. Rev. Lett. **76**(16), 2926–2929 (1996).

21. D. Ehrt, "Phosphate and fluoride phosphate optical glasses - Properties, structure and applications," Phys. Chem. Glasses B **56**(6), 217–234 (2015).

22. J. Ren, X. Xu, W. Shen, G. Chen, S. Baccaro, and A. Cemmi, "Gamma-ray induced reversibile photochromism of Mn2+ activate borophosphate glasses," Sol. Energy Mater. Sol. Cells **143**, 635–639 (2015).

23. G. Quian, S. Baccaro, A. Guerra, L. Xiaolan, G. Shuanglong, G. Iurlaro, and G. Chen, "Gamma irradiation effects on ZnO-based scintillating glasses containing CeO2 and/or TiO2," Nucl. Instrum. Methods Phys. Res. B **262**(2), 276–280 (2007).

24. F. Lei, R. R. Truscott, C. S. Dyer, B. Quaghebeur, D. Heynderickx, R. Nieminen, H. Evans, and E. Daly, "MULASSIS: a Geant4-based multilayered shielding simulation tool," IEEE Trans. Nucl. Sci. **49**(6), 2788–2793 (2002).

25. FASTRAD 3D radiation software, https://www.fastrad.net/ (last access in November 2018).

26. S. M. Seltzer, "Updated calculations for routine space-shielding radiation dose estimates: SHIELDOSE-2," NIST Publication NISTIR 5477, Gaithersburg, MD. (1994).

27. G. R. Wirtenson and R. H. White, "Effects of ionizing radiation on selected optical materials: an overview," Technical Report UCRL-ID-111453 (1992).